Two Birds with One Stone: High-Quality Utilization of COVID-19 Waste Masks into Bio-Oil, Pyrolytic Gas, and Eco-Friendly Biochar with Adsorption Applications

Tongtong Wang [1], **Di Zhang [2]**, **Hui Shi [1,2,*]**, **Sen Wang [3]**, **Bo Wu [2]**, **Junchao Jia [4]**, **Zhizhen Feng [4]**, **Wenjuan Zhao [4]**, **Zhangyue Chang [4] and Dalal Z. Husein [5,*]**

[1] Institute for Interdisciplinary and Innovate Research, Xi'an University of Architecture and Technology, Xi'an 710055, China; wangtongtong@xauat.edu.cn
[2] School of Environmental and Municipal Engineering, Xi'an University of Architecture and Technology, Xi'an 710055, China; dizhang@nwafu.edu.cn (D.Z.); wubo@xauat.edu.cn (B.W.)
[3] School of Resources Engineering, Xi'an University of Architecture and Technology, Xi'an 710055, China; wangsen@xauat.edu.cn
[4] Bio-Agriculture Institute of Shaanxi, Shaanxi Province Academy of Sciences, Xi'an 710043, China; jiajc@xab.ac.cn (J.J.); fengzz@xab.ac.cn (Z.F.); myszhwj@xab.ac.cn (W.Z.); changzy@xab.ac.cn (Z.C.)
[5] Chemistry Department, Faculty of Science, New Valley University, El-Kharja 72511, Egypt
*   Correspondence: shihui@xauat.edu.cn (H.S.); dalal_husein@sci.nvu.edu.eg (D.Z.H.)

Abstract: As a common necessity, masks have been used a lot in recent years, and the comprehensive utilization of waste masks has become a research priority in the post-COVID-19 pandemic era. However, traditional disposal methods suffer from a range of problems, including poor utilization and insecurity. To explore new solution ideas and efficiently utilize waste resources, waste masks and biomass wastes were used as raw materials to prepare mask-based biochar (WMB), bio-oil, and pyrolytic gas via oxygen-limited co-pyrolysis in this study. The obtained solid–liquid–gas product was systematically characterized to analyze the physicochemical properties, and the adsorption properties and mechanisms of WMB on the environmental endocrine bisphenol A (BPA) were investigated. The co-pyrolysis mechanisms were also studied in depth. Furthermore, the strengths and weaknesses of products prepared by co-pyrolysis and co-hydrothermal synthesis were discussed in comparison. The results indicated that the waste masks could shape the microsphere structure, leading to richer surface functional groups and stable mesoporous of WMB. Here, the risk of leaching of secondary pollutants was not detected. The theoretical maximum adsorption of BPA by WMB was 28.73 mg·g^{-1}. The Langmuir and Pseudo-second-order models optimally simulated the isothermal and kinetic adsorption processes, which are a composite of physicochemical adsorption. Simultaneous pyrolysis of mask polymers with biomass polymers produces bio-oil and pyrolytic gas, which is rich in high-quality aliphatic and aromatic compounds. This could have potential as an energy source or chemical feedstock. The co-pyrolysis mechanisms may involve the depolymerization of waste masks to produce hydrocarbons and H radicals, which in turn undergo multi-step cleavage and oligomerization reactions with biomass derivatives. It is recommended to use the co-pyrolysis method to dispose of waste masks, as the products obtained are significantly better than those obtained by the co-hydrothermal method. This work provides a new contribution to the resourcing of waste masks into high-quality products.

Keywords: waste masks; co-pyrolysis; biochar; bio-oil; pyrolytic gas; pollutant removal

1. Introduction

Before the outbreak of coronavirus disease 19 (COVID-19), air pollution from vehicle exhaust and industrial emissions became more prominent in many areas as global industrialization accelerated. With the improvement of medical standards, people's awareness

of respiratory protection gradually increased, in some places and cultures (e.g., in China), leading to the rapid development of the mask industry [1]. Following the global pandemic of COVID-19, the World Health Organization (WHO) and governments have begun to implement mandatory requirements for wearing disposable medical masks (DMMs) in public places to reduce the spread of the virus. This has led to a surge in the demand for DMMs from the year 2020 to 2023 [2,3]. According to research estimates, nearly 129 billion DMMs are consumed globally every month, with Asia (especially in China) recording the highest usage [4]. From March to December 2020 alone, China exported 224.2 billion DMMs as per the Chinese Customs statistics. With the arrival of the post-COVID-19 pandemic era, people around the world pay more attention to the protection of their safety, and DMMs have become an essential daily necessity for human life. The huge demand and usage resulted in the production of waste masks. At 3 g per waste mask, more than several hundred thousand tons of solid waste were produced during the COVID-19 pandemic alone [5]. Even, most of the waste masks are casually discarded, which may not only cause the spread of viruses but also seriously affect the health of the ecosystem [6]. Waste masks that enter the environment take 400–500 years to degrade naturally, and there is also a risk of releasing micro- or nanoplastics that may also enter the food chain, evolving this into a new type of hazardous solid waste [6,7]. Additionally, some studies have found that these waste masks have significant harmful effects on marine ecosystems, climate change, and soil [8]. Therefore, the effective treatment and comprehensive utilization of waste masks have become a research hotspot of global concern [9].

Common disposal methods for waste masks include high-temperature incineration and landfill degradation [5]. However, this may release secondary contaminants and result in a high risk of virus spread in multiple environmental media [3,6]. Therefore, chemical heat treatment to carbonize it based on mechanical and chemical recycling has been proposed, which is an easy, green, cheap, and reliable disposal method [7,8]. Specifically, the process mainly consists of oxygen-limited pyrolysis carbonization, (high-pressure) hydrothermal carbonization, and catalytic carbonization [9,10]. Moreover, DMMs essentially consist of polymers (e.g., polypropylene, polyester fibers) and metal nose clips [5], which implies that the carbon sources within them have the potential to be converted into carbon materials [7–9]. Moreover, carbonization of the mask polymers is typical of stoichiometric cleavage, where the breakage of the chemical bonds leads to the random production of a certain quantity of low-molecular-weight hydrocarbons [11]. It will produce bio-oils and pyrolytic gases [5–7]. Abbas-Abadi et al. [12] performed pyrolysis of polypropylene in a stirred autoclave reactor and achieved a polypropylene conversion of 99.6% at 450 °C. The liquid products of this process were mainly naphthenes, paraffins, olefins, and aromatics. Oginni et al. [13] discussed the possibility of converting DMMs into high value-added products and concluded that oxygen-limited pyrolysis is one of the important thermochemical conversion technologies. It was also elucidated mechanistically that DMMs allow the preparation of carbon materials and the simultaneous obtaining of bio-oil and pyrolytic gas. Moreover, the hydrothermal reaction provides high pressure, and this carbonization process not only reduces energy consumption but also enhances the high value-added of the liquid [10]. However, the current research mainly focuses on pyrolysis carbonization and catalytic carbonization, while hydrothermal carbonization is not sufficiently studied [5–7]. As a new approach, co-pyrolysis or co-hydrothermal reaction in the carbonization of mask polymers is even more sparsely studied. Emenike et al. [14] suggested the preparation of biochar by co-pyrolysis of waste masks and leaves, which is recommended as an adsorbent or soil fertilizer. Additionally, the solid, liquid, and gaseous substances produced by this co-pyrolysis process are defined as biochar, bio-oil, and pyrolytic gas, respectively [7,9,12]. However, this cannot help but confuse scholars: Bio-oil and pyrolytic gas are also produced during the co-pyrolysis for mask-based biochar preparation, and what are their chemical compositions? It is notable that, "bio-oil" and "biochar" terms are commonly used to describe hydrocarbon materials and char that are produced during the pyrolysis process regardless the source is natural biomass or synthetic materials [15]. The similarities and

differences with published reports still need to be discussed to clarify the potential value of bio-oil and pyrolytic gas. Moreover, the role played by discarded masks in the structure of materials and the adsorption properties of mask-based biochar remain unclear. The riskiness of mask-based biochar in environmental applications is also worth exploring. Even, what is the effect of co-pyrolysis and co-hydrothermal reaction on the comprehensive utilization of waste masks? A comparative exploration is needed.

In this study, it is suggested to select bisphenol A (BPA, $C_{15}H_{16}O_2$) as a representative pollutant for endocrine disruptors that are widely used in plastics, food, and fine chemicals [16]. Endocrine disruptors are chemicals that can disrupt endocrine function and affect the regulation of hormones in the body, such as phthalates, polychlorinated biphenyls, dioxins, and BPA. As an emerging environmental pollutant, BPA is detected in surface water, groundwater, and even drinking water [17]. The residual liquid of BPA entering organisms may cause endocrine system disruption and hazardous to human health, and adsorption is a cost-effective and feasible treatment method [18]. Moreover, it highlights the urgency of current efforts to control environmental endocrine disruptors, such as BPA. Therefore, the main research objectives of this work included (1) preparation of waste mask-based biochar (WMB) from waste masks and waste biomass (e.g., cow dung) by co-pyrolysis in an oxygen-limited atmosphere. Advanced characterization techniques were used to analyze the basic physicochemical properties of the prepared materials and the role of DMMs in the material structure. (2) The chemical compositions of bio-oil and pyrolytic gas produced in the co-pyrolysis were analyzed in depth, and the high value-added products and co-pyrolysis mechanisms were discussed in comparison to highlight this work. (3) The batch adsorption experiments of BPA by WMB were systematically investigated, and the experimental data were fitted using four isothermal adsorption and four adsorption kinetic models to elucidate the adsorption characteristics. (4) Preparation of hydrothermal waste mask-based carbon (HWMB) by co-hydrothermal synthesis, together with the by-product hydrothermal bio-oil. The advantages and disadvantages of the products prepared by co-pyrolysis and co-hydrothermal synthesis were discussed to reveal the differences. Finally, the risk of environmental applications was evaluated. This study is in line with the green development concept of "killing two birds with one stone, treating waste with waste". In other words, this study is about the efficient conversion of waste masks into valuable by-products (bio-oil and pyrolytic gas) and biochar, where biochar is then used to treat the emerging pollutant BPA. This is in line with the United Nations Sustainable Development Goals and the concept of a circular economy. It is expected to expand new ideas for the comprehensive utilization of waste masks and the preparation of environmentally functional materials and also provide a theoretical basis for obtaining high value-added bio-oil and pyrolytic gas products.

2. Materials and Methods

2.1. Materials

All solvents and chemicals are analytically pure and purchased from China National Pharmaceutical Group Chemical Reagent Co. (Beijing, China). Ultrapure water will be used throughout the experiments. Waste masks (mainly composed of polypropylene and polyester fibers) and cow dung used in this study were collected from supermarkets or a dairy in Xi'an City.

2.2. Biochar and By-Products

Weighing 10 g of dried waste masks and 20 g of cow dung were mixed well in an alumina crucible and put into a box-type atmosphere furnace with nitrogen for co-pyrolysis. The multi-stage program heating was adopted, and the pyrolysis temperature was set at 450 °C, the constant temperature time was 3 h, and the heating rate was 2.5 °C·min^{-1}; the reaction was naturally cooled to room temperature after the end of the reaction. Subsequently, the solid obtained was ground through an 18-mesh sieve, i.e., mask-based biochar, abbreviated as WMB. Also, the control materials, i.e., the pure mask biochar (PMB) and

the pure cow dung biochar (PCB), were prepared according to the same conditions. The biochar was simply activated by ultrasound in a KQ-300ES constant temperature numerically controlled ultrasonic machine (Kunshan Ultrasonic Instrument Co., Ltd., Kunshan, China) to remove impurities. The bio-oil and pyrolytic gas were collected by a condensing reflux device and a green aluminum foil air harvesting bag. The preparation process is shown in Figure 1. The same ratio of waste masks and cow dung was weighed into a Teflon™-equipped autoclave (SLM 250, Beijing Sen Long Reactor Co., Ltd., Beijing, China) with a controlled fill ratio of ~60% and hydrothermally reacted at 220 °C for 10 h (with stirring). Finally, it is cooled to room temperature to obtain HWMB and the co-hydrothermal bio-oil; similarly, preparation of control materials, pure waste mask hydrothermal carbon (HMB), and the corresponding hydrothermal bio-oil.

Figure 1. Schematic illustration of the preparation process in this study.

2.3. Characterization

The surface morphology of the biochar samples was analyzed in a Sigma HD scanning electron microscope (SEM, Carl Zeiss AG, Oberkochen, Germany) at a 2.0 kV, which was loaded with an X-MAXEDS Energy-Dispersive Spectrometer (EDS, Oxford Instruments, Oxford, UK). The BET Specific surface area (S_{BET}) and pore size analysis were determined using N_2 as the adsorbate at 77 K and relative pressure of 0.05–0.20, for which an ASAP2460 plus analyzer (Micromeritics Instruments Co., Norcross, GA, USA) was used. The mineral species were identified using a D-MAX 2500 X-ray powder diffractometer (XRD, Rigaku Co., Ltd., Wilmington, NC, USA). The measurements were performed at a 0.02 scan step size, 2 deg·min^{-1} scan speed, 0.15 receiving slit width, 30–40 kV, and 30–40 mA. The infrared spectra (FTIR) were measured with KBr pellet methods using a Vertex70 FTIR spectrometer (Bruker Co., Ltd., Billerica, MA, USA) over a range of 400~4000 cm^{-1} with a resolution of 2 cm^{-1}. The gas chromatography–tandem mass spectrometer (GC-MS, Agilent 7890A/7000B GC-QQQ, Santa Clara, CA, USA) was used to analyze the components of bio-oil and pyrolytic gas. Meanwhile, matching analyses were performed based on the NIST.17 mass spectrometry database [19–21].

2.4. Batch Experiments

The BPA solution contained 1 mL of anhydrous ethanol as a solvent to dissolve completely at room temperature (25 °C), and the pH of the solution was adjusted to approximately neutral with dilute NaOH and dilute HCl. Adequate conical flasks were taken, and 50 mL of 10 mg·L^{-1} of BPA solution and 0.05 g of the materials were added separately and placed in a gas-bath thermostatic oscillator for 24 h at 240 rpm at room temperature. The mixture was centrifuged at high speed for solid–liquid separation. Three parallel replicates were assigned to each treatment, together with control and blank treatments, and statistical methods were applied to take the mean values for subsequent

analysis. BPA concentration was determined on a Shimadzu Nexera UHPLC LC-30A ultra-high-performance liquid chromatography (Kyoto, Japan). The adsorption capacity (Q_e, mg·g^{-1}) and removal rate (R_e, %) at equilibrium were calculated as follows:

$$Q_e = (C_0 - C_e)\frac{V}{m} \tag{1}$$

$$R_e = (1 - \frac{C_e}{C_0}) \times 100\% \tag{2}$$

where C_0 and C_e are the initial and equilibrium concentrations (mg·L^{-1}), respectively. m is the mass of added the materials (g), and V is the solution volume (L). (1) Isothermal adsorption: The initial BPA concentrations were established at 1, 5, 10, 15, 20, 30, 40, 50, and 100 mg·L^{-1}, respectively. (2) Adsorption kinetics: the adsorption times of BPA were established at 5, 10, 20, 30, 60, 180, 300, 600, 900, 1200, 1440, and 2880 min, respectively. Other settings were the same as the batch experiment above.

2.5. Adsorption Models and Data Analysis

To better investigate the adsorption characteristics, four isotherms models (Langmuir, Freundlich, Temkin, and Dubinin–Radushkevich) and four adsorption kinetic models (Pseudo-first-order, Pseudo-second-order, Elovich, and Intraparticle diffusion) were used in Table S1 [20]. Isothermal adsorption and adsorption kinetic curves were fitted and plotted using OriginPro 2018b (OriginLab, Northampton, MA, USA).

3. Results and Discussions

3.1. Characterization

3.1.1. Microscopic Morphology and Elemental Analysis

Figure 2a clearly shows that the PMB is composed of many irregularly shaped particles, which may be ester substances produced by the polymer pyrolysis reaction of the waste mask. The blocky and cubic particles scattered on the surface may be crystals of polypropylene, a component of waste masks [5,14]. Figure 2b shows that there are fiber textures and pores on the surface of PCB, and it contains impurity particles, which is a typical biochar material. Figure 2c shows that the WMB surface contains both fibrous structures from biomass and also clearly visible micro-spherical or block-like protrusions. These spherical protrusions are likely formed by the co-pyrolysis of natural polymers (cellulose, hemicellulose, and lignin) in the biomass and the mask polymer and are widely distributed on the surface of WMB (Figure 2d). This means that the polymers introduced by the waste masks, such as polypropylene and polyester fibers, affect the entire structure of the biochar through thermal polymerization and pyrolysis, shaping a microspherical structure [9]. The surface elemental data of the prepared materials were analyzed by EDS and are summarized in Table 1. With the co-pyrolysis of waste masks and biomass, the C content of WMB was significantly higher than that of PMB and PCB, but the O and N contents were significantly lower. This indicates that co-pyrolysis with biomass facilitates the carbonization of waste masks.

Table 1. Basic physicochemical properties of the prepared biochar.

Biochar Type	C (%) [a]	N (%)	O (%)	P (%)	S (%)	S_{BET} (m^2·g^{-1})	Pore Volume [b] (cm^3·g^{-1})	Pore Size [c] (nm)
PMB	37.98	1.02 [d]	59.02	1.55	0.43	- [d]	-	-
PCB	61.88	5.09	24.97	3.24	2.84	9.42	0.009	14.91
WMB	78.98	1.72	14.97	1.56	0.60	30.85	0.015	8.81

[a] These data are from EDS energy spectra. [b] Single point adsorption total pore volume. [c] Adsorption average pore diameter (4V/S_{BET}). [d] "-" means have not been detected or not determined.
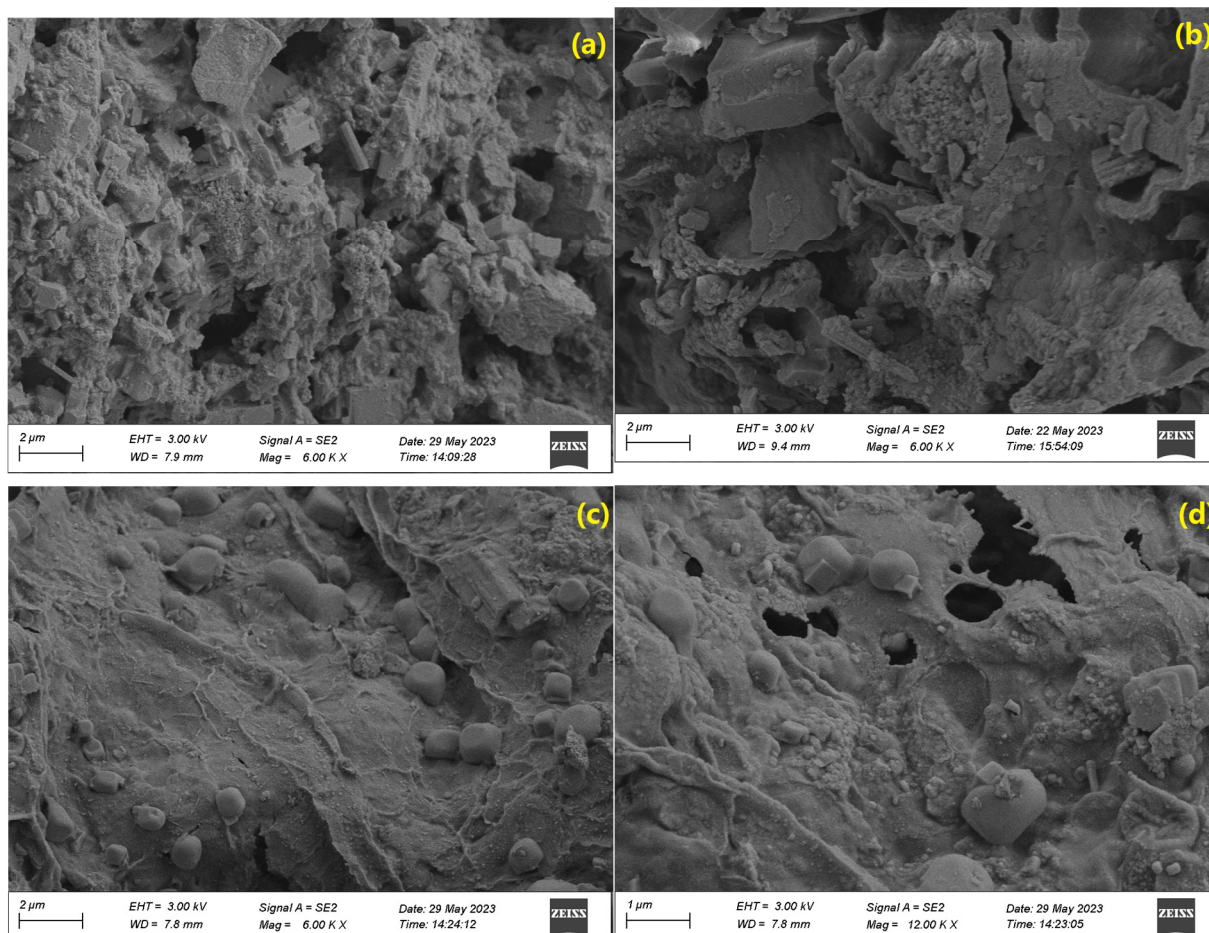
Figure 2. SEM images of the prepared biochar: (**a**) for PMB (magnified 6000 times), (**b**) for PCB (magnified 6000 times), (**c**) for WMB (magnified 6000 times), and (**d**) for WMB (magnified 12,000 times).

3.1.2. Specific Surface Area and Pore Size Analysis

According to the International Union of Pure and Applied Chemistry (IUPAC), PMB is not a mesoporous material (Table 1). However, PCB and WMB are mesoporous materials, as their average pore size is between 2 and 50 nm [21]. Moreover, with the introduction of waste masks, the BET-specific surface area (S_{BET}) and pore volume of WMB increased significantly, and the average pore diameter decreased. Figure S1a also shows that the adsorption–desorption curve of WMB follows type IV and has a significant hysteresis loop, which confirms that it is a mesoporous material [22]. Figure S1b indicates that the pore size of WMB is mainly distributed between 2 and 15 nm. Figure S1c explains that the cumulative pore volume and pore area of WMB decrease with increasing average pore diameter. Thus, these characterization data suggest that WMB acts as a carbon-based adsorbent.

3.1.3. XRD and FTIR Analysis

XRD diffraction patterns are shown in Figure 3a to analyze the phase structure of the prepared materials. Using the Jade 6.5 software and the International Crystal Database (ICDD) standard material card analysis, it was found that these materials all have a distinct diffraction peak at 2θ = 26.4°, and the crystal was matched to a carbon framework (JCPDS № 26-1080). This may mean that PMB, PCB, and WMB are all carbonized through pyrolysis. Compared to the diffraction pattern of the PCB, which contains many noisy signals, the WMB prepared by the co-pyrolysis method better matches the diffraction peaks of various crystals. This also includes polypropylene (JCPDS № 47-1952), polyethylene (JCPDS № 53-

1859), polyethylene terephthalate (JCPDS № 50-2275), and ketone-like peaks, which come from waste masks. The XRD spectra prove that the waste masks undergo further thermal chemical reactions with the biomass during co-pyrolysis, thereby enhancing the crystalline properties of the surface [5,14]. This also supports the SEM analysis results above, which show that the microspheres may be composed of polymers (such as polypropylene) and ester crystals.
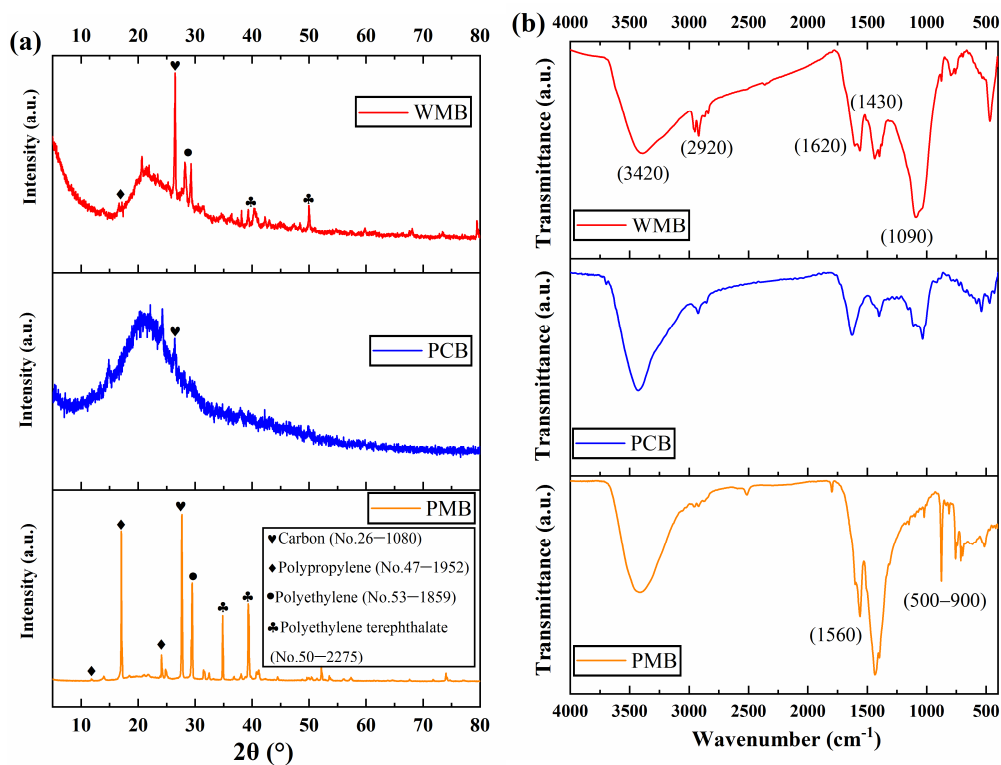

Figure 3. XRD and FTIR analysis of the prepared biochar: (**a**) for XRD and (**b**) for FTIR.

The FTIR spectra are shown in Figure 3b (processed with baseline correction) and were used to analyze the surface functional groups of the prepared materials. Overall, these prepared materials have similar characteristic peaks, including hydroxyl (-OH) stretching vibration peaks near 3420 cm^{-1}, C-H stretching vibration peaks (such as methyl -CH$_3$) near 2920 cm^{-1}, amino (-NH$_2$) resonance peaks near 1620 cm^{-1}, aromatic acid -COOH resonance peaks near 1560 and 1430 cm^{-1}, C-C/C=C resonance peaks near 1090 cm^{-1}, and aromatic compounds and other heterocyclic functional groups near 500–900 cm^{-1} [20–22]. With the co-pyrolysis of waste masks and biomass, the -OH stretching vibration peak (3420 cm^{-1}) and the C-C/C=C resonance peak (1090 cm^{-1}) are significantly enhanced; however, the -COOH vibration peak near 1560 and 1430 cm^{-1} is significantly weakened. This indicates that the mask polymer and biomass polymer undergo a cleavage reaction, significantly enhancing carbonization [5,6], attributed to the tendency of -COOH to convert to -OH and C-C/C=C. Furthermore, aromatic or heterocyclic compounds in the range of 500 to 900 cm^{-1} are further converted to esters, ketones, or hydrocarbons by co-pyrolysis. This suggests that the co-pyrolysis method for disposing of waste masks is more thorough than the carbonization process of pyrolysis alone.

3.2. Analysis of Bio-Oils

GC-MS was used to analyze the bio-oils produced during individual pyrolysis and co-pyrolysis. About 52 chromatographic peaks were identified in the pyrolysis process of pure waste masks, which included 30 compounds. A total of 83 peaks were identified in the co-pyrolysis of waste masks and biomass, including 61 compounds. These data are collated in Table 2, with compounds selected based on matching degree and peak area

greater than 0.5. It could be found that the ester compounds are the most abundant in this bio-oil (corresponding to PMB), with a peak area of over 40%, followed by aliphatic and heterocyclic compounds. The highest content was 1,4-benzenedicarboxylic acid, bis(2-ethylhexyl) ester, as high as 33.87%. This is a common plasticizer that is added to polyvinyl chloride (PVC) products such as pipes, flooring, and wallpaper to increase their flexibility and plasticity. Additionally, some alkanes, ethers, and furans are also contained, but in lower concentrations and with lower availability. This is due to the breakage of the polymer chains and the polycondensation reaction in the mask polymers (polypropylene and polyester). Li et al. [23] also concluded that the products of pyrolysis of DMMs without catalysis are mainly alcohols, alkanes, ethers, esters, and fluorides.

Table 2. The main components of bio-oils were analyzed via GC-MS.

Corresponding Biochar Type	№	Library/ID	CAS №	Chemical Formula	Ret. Time (min)	Peak Area (%)
PMB	1	1,4-Benzenedicarboxylic acid, bis(2-ethylhexyl) ester	6422-86-2	$C_{24}H_{38}O_4$	29.196	33.87
	2	Phthalic acid, di(2-propylpentyl) ester	- [a]	$C_{24}H_{38}O_4$	27.434	1.69
	3	Furan-2-carbonyl chloride, tetrahydro-	52449-98-6	$C_5H_7ClO_2$	6.759	1.51
	4	Pentanoic acid, 4-oxo-, ethyl ester	539-88-8	$C_7H_{12}O_3$	6.500	1.33
	5	Heptanediamide, N,N′-di-benzoyloxy-	-	$C_{21}H_{22}N_2O_6$	8.218	1.21
	6	3,3-Diethoxy-1-propanol, propyl ether	-	$C_{10}H_{22}O_3$	7.099	1.07
	7	Hexadecanoic acid, ethyl ester	628-97-7	$C_{18}H_{36}O_2$	21.554	0.84
	8	Eicosane, 2-methyl-	1560-84-5	$C_{21}H_{44}$	10.633	0.80
	9	Furan, 2,5-diethoxytetrahydro-	3320-90-9	$C_8H_{16}O_3$	5.789	0.74
	10	Dibutyl phthalate	84-74-2	$C_{16}H_{22}O_4$	21.254	0.57
	11	p-Xylene	106-42-3	C_8H_{10}	3.667	0.52
	12	Decane, 2,4,6-trimethyl-	62108-27-4	$C_{13}H_{28}$	6.340	0.50
WMB	1	1,6-Heptadien-4-ol	2883-45-6	$C_7H_{14}O$	6.745	12.75
	2	Phenol	108-95-2	C_6H_6O	5.351	6.59
	3	Benzoic acid	65-85-0	$C_7H_6O_2$	8.259	5.45
	4	o-Acetyl-L-serine	5147-00-2	$C_5H_9NO_4$	6.415	2.65
	5	Phenol, 2-methoxy-	90-05-1	$C_7H_8O_2$	6.922	2.10
	6	Ethoxyacetaldehyde diethylacetal	4819-77-6	$C_8H_{18}O_3$	4.531	1.95
	7	Butyrolactone	96-48-0	$C_4H_6O_2$	4.344	1.94
	8	Pentanoic acid, 4-oxo-, ethyl ester	539-88-8	$C_7H_{12}O_3$	6.490	1.49
	9	Propanoic acid, 2-hydroxy-, ethyl ester, (L)-	687-47-8	$C_5H_{10}O_3$	3.106	1.46
	10	3-Mercaptohexyl hexanoate	136954-22-8	$C_{12}H_{24}O_2S$	8.177	1.37
	11	2-Cyclopenten-1-one, 2-hydroxy-3-methyl-	80-71-7	$C_6H_8O_2$	5.983	1.28
	12	2-Diethoxymethyl-3-methyl-butan-1-ol	-	$C_{10}H_{22}O_3$	10.228	1.11
	13	3,3-Diethoxy-1-propanol, propyl ether	-	$C_{10}H_{22}O_3$	7.096	1.02
	14	4-Nonanol, 4-methyl-	23418-38-4	$C_{10}H_{22}O$	9.133	0.98
	15	2-Cyclopenten-1-one	930-30-3	C_5H_6O	3.348	0.94
	16	2-Cyclopenten-1-one, 2-hydroxy-	10493-98-8	$C_5H_6O_2$	4.490	0.83
	17	4-Methoxy-1-pentene	98386-09-5	$C_6H_{12}O$	4.225	0.75
	18	2-Ethoxytetrahydrofuran	13436-46-9	$C_6H_{12}O_2$	3.174	0.74
	19	Butanedioic acid, diethyl ester	123-25-1	$C_8H_{14}O_4$	8.504	0.74
	20	2-Cyclopenten-1-one, 3-methyl-	2758-18-1	C_6H_8O	5.086	0.73
	21	3,3-Diethoxy-1-propanol, butyl ether	-	$C_{11}H_{24}O_3$	5.779	0.69
	22	Diethoxymethyl acetate	14036-06-7	$C_7H_{14}O_4$	3.011	0.61
	23	Glycerol triethyl ether	162614-45-1	$C_9H_{20}O_3$	4.099	0.59
	24	Hexadecanoic acid, ethyl ester	628-97-7	$C_{18}H_{36}O_2$	21.554	0.54
	25	2-Cyclopenten-1-one, 2,3-dimethyl-	1121-05-7	$C_7H_{10}O$	6.157	0.50
	26	2-Propanol, 1,1-dimethoxy-	42919-42-6	$C_5H_{12}O_3$	4.184	0.50

[a] This means the default CAS data.

Table 2 also shows that the composition of the bio-oil obtained by co-pyrolysis is significantly richer than that of the bio-oil mentioned above (by pyrolysis alone). The most abundant are aliphatic compounds, with a relative peak area content of over 32%

and a proportion of over 60%. These mainly include alkanes, alkenes, alcohols, amides, fatty acids, aldehydes, etc. These substances usually have combustion characteristics and a calorific value, so they can be used as potential fuels such as biodiesel. Moreover, heterocyclic and aromatic compounds, with relatively low content of about 8.69% and 5.45%, respectively, were also detected. The most abundant of these compounds is 1,6-Heptadien-4-ol, which accounts for 12.75%. 1,6-Heptadien-4-ol is a colorless liquid with a phenol-like aromatic odor. It is used as a chemical product in perfumes, paints, synthetic resins, nonionic surfactants, etc. It can also be used as a synthetic intermediate for certain drugs, such as anti-tumor and anti-depressant drugs. Furthermore, the relatively high content of phenol, benzoic acid, and o-acetyl-L-serine is also a very important and versatile chemical raw material with broad application prospects in the pharmaceutical and food industries. Furthermore, this means that the co-pyrolysis of waste masks and biomass not only increases the production of aliphatic compounds but also reduces heterocyclic and aromatic compounds with low utilization value, increasing the added value of the bio-oil.

3.3. Analysis of Pyrolytic Gases

Similarly, 189 peaks were identified in the pyrolytic gas of the pure waste masks (by pyrolysis alone), including 131 compounds. A total of 98 peaks were identified in the co-pyrolysis of waste masks and biomass, including 57 compounds. These data were collated in Table 3, with compounds selected based on matching degree and peak area greater than 1.0. Overall, the pyrolytic gas components from PMB are more varied and complex than the bio-oil components, which mainly include alkanes, heterocyclic compounds, and CO_2. The highest content is ethyne, fluoro-, with a peak area of about 15.21%, followed by carbamic acid, monoammonium salt, and CO_2, with peak areas of 10.53 and 9.23, respectively. Carbamic acid and monoammonium salt may produce nitrogen oxides and ammonia when burned at high temperatures. This indirectly indicates that the pyrolysis alone is mainly due to the conversion of polypropylene to ethyne, fluorine, and CO_2. Carbamic acid and monoammonium salt may come from the pyrolysis of nitrogen-containing dyes in pure waste masks. However, there is a clear difference from the report by Li et al. [23], who suggested that the gas products were mainly H_2, CO, CO_2, CH_4, and C_2H_4. This may be related to this study using an oxygen-limited pyrolysis process without hydrocracking. Secondly, it may also be related to the detection method and the matching mass spectral database.

It can be found that the pyrolytic gas produced from WMB mainly includes aliphatic compounds (such as amines, alcohols, and esters), heterocyclic compounds, a few aromatic compounds, and CO_2. Among them, the highest content is (2-Aziridinylethyl)amine, with a peak area of about 23.72%. This may be a product of condensation of pyrolytic gases and is often used as an organic synthesis agent, buffer, and surfactant. In organic synthesis, it can be used as a catalyst for compounds such as hydrazine, amino acid reagents, mercaptans, and carboxylic acids to promote chemical reactions. Secondly, 1,2,4-Benzenetricarboxylic acid, 1,2-dimethyl ester (20.35%), and D-Allose (8.65%) are also relatively high in content. They can be used as industrial raw materials and applied in the manufacture of polyester resins, plastics, pharmaceuticals, etc. However, the co-pyrolysis produces pyrolytic gas with a very low CO_2 content, which may mean that the waste masks have undergone sufficient pyrolysis conversion with the biomass. In this process, the pyrolytic gas contains fewer non-valuable components (CO_2 or volatile organic pollutants) than the pyrolysis alone. Moreover, in combination with the analysis of the bio-oil composition described above, it can be seen that co-pyrolysis is more resource-efficient and has a higher added value.

Table 3. The main components of pyrolytic gases were analyzed via GC-MS.

Corresponding Biochar Type	№	Library/ID	CAS №	Chemical Formula	Ret. Time (min)	Peak Area (%)
PMB	1	Carbamic acid, monoammonium salt	1111-78-0	$CH_6N_2O_2$	1.024	8.38
	2	3-Pyridinol	109-00-2	C_5H_5NO	9.492	4.82
	3	D-Allose	2595-97-3	$C_6H_{12}O_6$	18.855	4.42
	4	Carbon dioxide	124-38-9	CO_2	1.132	4.34
	5	Carbon dioxide	124-38-9	CO_2	1.098	3.06
	6	1,6-Anhydro-β-d-talopyranose	- [a]	$C_6H_{10}O_5$	16.431	2.36
	7	D-Allose	2595-97-3	$C_6H_{12}O_6$	18.818	2.15
	8	Carbamic acid, monoammonium salt	1111-78-0	$CH_6N_2O_2$	0.959	2.15
	9	Ethyne, fluoro-	2713-09-9	C_2HF	1.439	2.13
	10	Ethyne, fluoro-	2713-09-9	C_2HF	1.541	1.89
	11	D-Allose	2595-97-3	$C_6H_{12}O_6$	18.729	1.88
	12	Carbon dioxide	124-38-9	CO_2	1.187	1.83
	13	Ethyne, fluoro-	2713-09-9	C_2HF	1.282	1.66
	14	Ethyne, fluoro-	2713-09-9	C_2HF	1.241	1.56
	15	Ethyne, fluoro-	2713-09-9	C_2HF	1.496	1.48
	16	Ethyne, fluoro-	2713-09-9	C_2HF	1.221	1.48
	17	Ethyne, fluoro-	2713-09-9	C_2HF	1.785	1.46
	18	Ethyne, fluoro-	2713-09-9	C_2HF	1.333	1.38
	19	3,5-Decadien-7-yne, 6-t-butyl-2,2,9,9-tetramethyl-	-	$C_{18}H_{30}$	30.626	1.35
	20	Amberonne (isomer 1)	-	$C_{16}H_{26}O$	30.599	1.19
	21	β-D-Glucopyranoside, methyl 3,6-anhydro-	3056-46-0	$C_7H_{12}O_5$	15.539	1.18
	22	Ethyne, fluoro-	2713-09-9	C_2HF	1.364	1.09
	23	Ethyne, fluoro-	2713-09-9	C_2HF	1.262	1.08
	24	3-O-Methyl-d-glucose	-	$C_7H_{14}O_6$	16.131	1.04
	25	Tetrapentacontane, 1,54-dibromo-	-	$C_{54}H_{108}Br_2$	30.936	1.03
	26	3,4-Altrosan	-	$C_6H_{10}O_5$	18.835	1.02
WMB	1	(2-Aziridinylethyl)amine	4025-37-0	$C_4H_{10}N_2$	1.092	23.72
	2	1,2,4-Benzenetricarboxylic acid, 1,2-dimethyl ester	54699-35-3	$C_{11}H_{10}O_6$	1.445	20.35
	3	D-Allose	2595-97-3	$C_6H_{12}O_6$	18.723	6.55
	4	1,6-Anhydro-β-d-talopyranose	-	$C_6H_{10}O_5$	16.311	2.47
	5	D-Allose	2595-97-3	$C_6H_{12}O_6$	18.672	2.10
	6	4a,7b-Dihydroxy-3-(hydroxymethyl)-1,1,6,8-tetramethyl-9a-((2-methylpropanoyl)oxy)-5-oxo-1a,1b,4,4a,5,7a,7b,8,9,9a-decahydro-1H-cyclopropa[3,4]benzo[1,2-e]azulen-9-yl 2-methylbutanoate	92214-55-6	$C_{29}H_{42}O_8$	31.916	1.88
	7	3-Pyridinol	109-00-2	C_5H_5NO	9.513	1.62
	8	Hydroquinone	123-31-9	$C_6H_6O_2$	14.499	1.28
	9	3-Pyridinol	109-00-2	C_5H_5NO	9.462	1.24
	10	Dasycarpidan-1-methanol, acetate (ester)	55724-48-6	$C_{20}H_{26}N_2O_2$	31.354	1.12

[a] This means the default CAS data.

3.4. Adsorption Application

The comparison of the adsorption capacity of BPA between WMB and the control material is shown in Figure S2. It can be seen that the adsorption capacity of BPA gradually increases with the increasing adsorption time until equilibrium is gradually reached at 1440 min. At equilibrium, the adsorption capacity of WMB for BPA was significantly higher than that of the control material, about 1.6 times. This indicates that the adsorption performance of the carbon materials prepared by co-pyrolysis is better than that of the carbon materials PMB and PCB prepared by pyrolysis alone, suggesting the advantages of co-pyrolysis in the disposal of waste masks.

Figure 4a shows the isothermal adsorption fitting curve of BPA by WMB. As the equilibrium concentration of BPA increases, the adsorption capacity of WMB gradually increases, showing a trend of first increasing and then stabilizing. The fitting results of the four classic isothermal adsorption models are given in Table 4. It can be seen that the fitting R^2 of the Langmuir, Freundlich, and Temkin models is greater than 0.95, which is significantly higher than that of the D-R model. Langmuir has the highest fitting R^2, indicating that the adsorption process is mainly monolayer adsorption. The Langmuir model calculated the theoretical maximum adsorption capacity of BPA by WMB as 28.726 mg·g^{-1}, which is similar to the maximum adsorption capacity obtained from the experiment, indicating a good fitting effect. The R^2 of the Temkin model is slightly greater than that of the Freundlich model, indicating that the adsorption process may involve chemical adsorption [18]. Moreover, in the Freundlich model, n = 1.636 < 2, indicating that the adsorption strength of BPA by WMB is not high and there is a risk of desorption [20]. In the D-R model, the adsorption energy of BPA on WMB is 0.128 kJ·mol^{-1}, indicating that the adsorption may be dominated by physical forces [22].

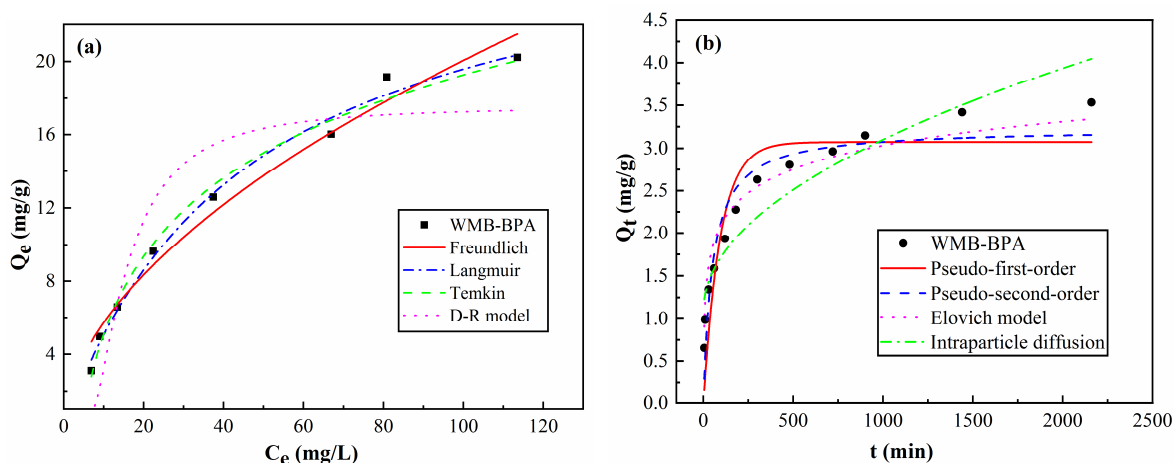**Figure 4.** Isotherm adsorption (**a**) and adsorption kinetics (**b**) of BPA by WMB.

Table 4. Adsorption model fitting parameters of BPA by WMB.

Langmuir			Freundlich			Temkin			D-R model		
a	Q_m/mg·g^{-1}	R^2	K_F	n	R^2	A	B	R^2	Q_0/mmol·g^{-1}	E/kJ·mol^{-1}	R^2
0.0214	28.726	0.991	1.636	1.837	0.972	0.229	6.154	0.988	17.577	0.128	0.833
Pseudo-first-order			Pseudo-second-order			Elovich			Intraparticle diffusion		
Q_e/mg·g^{-1}	k_1	R^2	Q_e/mg·g^{-1}	k_2	R^2	a	b	R^2	k_i	C	R^2
3.072	0.025	0.820	3.230	0.006	0.943	0.762	2.490	0.896	0.064	1.086	0.874

Figure 4b and Table 4 show the kinetic fitting curve of BPA adsorption by WMB and the relevant parameters, respectively. It could be found that the pseudo-second-order kinetic model has a high fitting degree of R^2, which explains the kinetic process of BPA adsorption by WMB well. The adsorption rate constant is 0.006 g·mg^{-1}·min^{-1}. Moreover, the maximum adsorption capacity fitted by the pseudo-second-order kinetic model is closer to the experimental value than that fitted by the pseudo-first-order kinetic model. The pseudo-second-order adsorption kinetic model can fully describe the adsorption process, including external liquid film diffusion, surface adsorption, and intra-particle diffusion [21]. This means that the adsorption process can be considered to involve both physical and chemical adsorption, which more realistically reflects the adsorption kinetic mechanism of BPA by WMB. The Elovich model fitting results show that the WMB surface has a uniformly

distributed adsorption energy, and the desorption constant b (2.490) is significantly greater than the adsorption constant a (0.762). This is consistent with the results of the isothermal adsorption model analysis. The adsorption of BPA by WMB is not stable and desorption is likely to occur [22]. The results of the fitting of the intra-particle diffusion model indicate that particle diffusion is not the only rate-limiting factor [20]. In combination with the best model, surface adsorption and liquid film diffusion also participate in controlling the adsorption rate of BPA. Additionally, the boundary layer coefficient C of WMB is 1.086, indicating that the boundary layer has a certain effect on the adsorption of BPA [21].

3.5. Co-Pyrolysis and Adsorption Mechanisms

3.5.1. Co-Pyrolysis Mechanisms

The main component of the waste masks used in this study is polypropylene, and it is generally believed that the pyrolysis mechanism of polypropylene is a free radical reaction. This mainly includes two stages: thermal initiation and chain-breaking [24]. During the thermal initiation stage, polypropylene is randomly cleaved by heat to produce alkyl radicals with different molecular weights. During the chain-breaking stage, alkyl radicals undergo a β-scission reaction to form an alkene and an alkyl radical with an unsaturated double bond. The alkene undergoes an intramolecular hydrogen transfer reaction with a macromolecule to form an alkyl radical. The alkyl radical with an unsaturated double bond undergoes a β-scission reaction to form a diene and, finally, two small-molecule radicals combine to form a chain terminator [25,26]. Moreover, Cheng et al. [27] believed that the main reaction is the dissociation of C-C bonds, producing small radical intermediates. Furthermore, the chain scission, recombination, isomerization, cyclization, and Diels–Alder reactions may occur.

Biomass, which consists of natural polymers such as hemicellulose, cellulose, and lignin, is pyrolyzed in a process that combines these three main components. As the pyrolysis temperature increases to about 105 °C, the water in the biomass begins to evaporate [28]. With the pyrolysis temperature continuing to increase, the hemicellulose begins to soften and undergo pyrolysis at 200–350 °C. Hemicellulose is a heterogeneous polymer composed of several different types of monosaccharides, accounting for 15–30% of the biomass. It is amorphous and has a branched structure. The pyrolysis process mainly includes the cleavage of glycosidic bonds, direct ring-opening of sugar units, dehydration of hydroxyl groups in the sugar ring, and dissociation of side chains [29]. The main products are carboxylic acids, non-aromatic ketones, and furans. Then, cellulose may undergo pyrolysis at 250–400 °C. Cellulose is a polymer composed of glucose units linked by β-(1-4) glycosidic bonds and usually accounts for 30–50% of the biomass. It is generally believed that the mechanism of cellulose pyrolysis is the formation of L-glucoside [30,31]. It is mainly divided into three stages: (1) the initial reaction stage (<300 °C), which is mainly the combination of water, the evaporation of free water, and the dehydration of hydroxyl groups. Meanwhile, it is depolymerized into low-molecular-weight active cellulose. (2) Glycosidic bond cleavage (primary depolymerization, 300–400 °C), with the main cleavage products including levoglucosan, pyran, and furan. (3) Secondary depolymerization (>400 °C), with the main products including furan compounds and small molecular oxygen-containing compounds [30]. Lignin, as an important component of lignocellulosic biomass, is mainly composed of coumarone, coniferyl alcohol, and sinapyl alcohol, which are connected by ether bonds and C-C bonds (5-5, β-1, and β-5) to form a three-dimensional network structure of high molecular substances, accounting for 5–20% of the biomass. Besides the ether bonds and C-C bonds between monomers, there are also various oxygen-containing functional groups, such as methoxy, carbonyl, and hydroxyl groups, which further increase the complexity of the lignin structure [32]. Finally, the pyrolysis of lignin mainly occurs at 160–900 °C. It mainly consists of three stages, namely, dehydration, devolatilization, and the breaking of strong chemical bonds [31–33]. At this stage, the alkaline functional groups and aromaticity of the biochar are enhanced [28], and the increasing volatiles and bio-oils make the pore structure of biochar more heterogeneous and uniform.

Furthermore, there is a positive synergistic effect between the co-pyrolysis of waste masks and biomass, as shown in Figure 5. The co-pyrolysis process promotes the formation of high-value bio-oil and biochar and reduces the production of low-value pyrolytic gas (which may contain polluting volatile gases). Hemicellulose and cellulose undergo dehydration, decarboxylation, deacidification, and secondary depolymerization to form furan compounds and lignin depolymerization to form phenolic compounds [31]. The depolymerization (random chain breakage) of waste masks produces a large number of aliphatic hydrocarbons (ethylene, propylene, 2-ene) and H radicals (H·) [34]. H·is provided to biomass-derived oxygenated compounds to promote the loss of hydroxyl, methoxy, and carbonyl groups, thereby reducing the oxygen content of the product. This increases the formation of aromatics, which in turn produces high-quality bio-oil and pyrolytic gas. Moreover, the pyrolysis of waste masks produces light olefins that undergo a Diels–Alder reaction with biomass-derived furan compounds to form aromatic hydrocarbons [35]. Studies have also shown that polypropylene-derived aliphatic hydrocarbons can provide hydrogen for biomass-derived oxygenated compounds, promote the formation of aromatics, and reduce the formation of coke [36]. Additionally, polypropylene-derived alkenes can be converted into light aromatics through reactions such as cyclization, aromatization, and low polymerization [31]. Similarly, furans derived from hemicellulose and cellulose, and phenols derived from lignin, are formed by dehydrogenation, decarboxylation, and oligomerization.
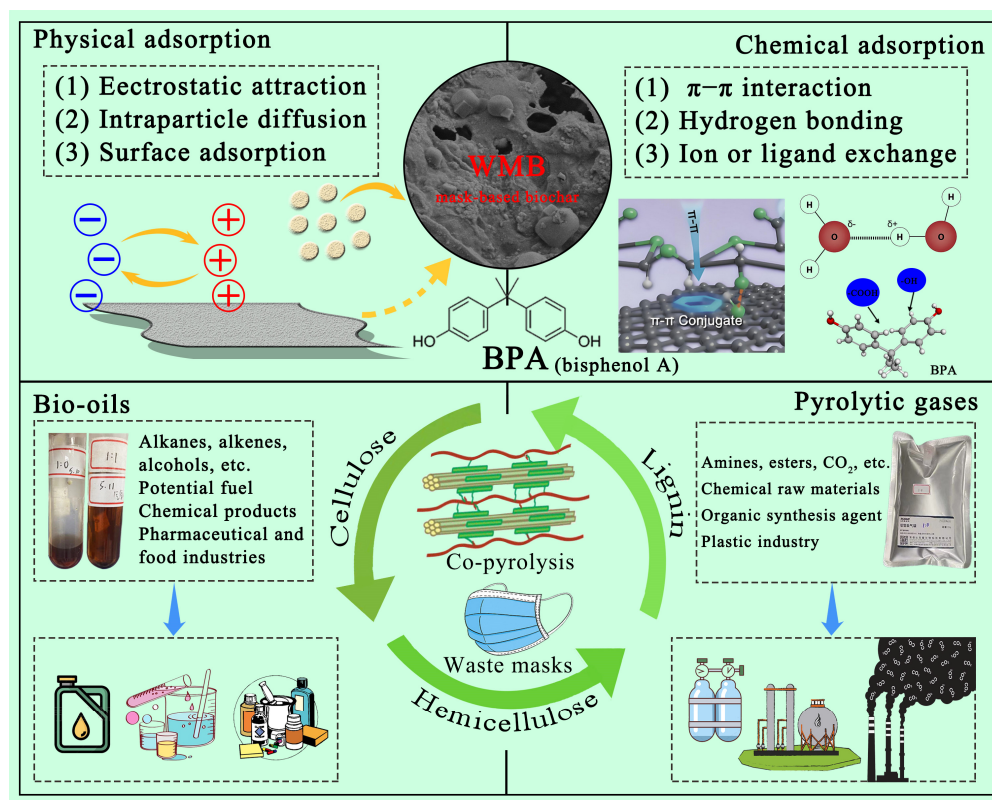

Figure 5. Schematic illustration of co-pyrolysis and adsorption mechanisms.

3.5.2. Adsorption Mechanisms

Exploring the adsorption mechanism of carbon materials can help promote their application in practical environments and provide new ideas for the design of new mask-based biochars. Based on the above experimental results and the analysis of the adsorption model, it can be inferred that the adsorption process of BPA by WMB involves both physical and chemical adsorption [37]. This is mainly due to the mesoporous structure, surface characteristics, rich surface functional groups, polar surface, and microsphere of WMB.

According to the best kinetic adsorption model, the second-order kinetic model, it can be inferred that the physical adsorption of BPA by WMB includes electrostatic adsorption, surface adsorption, intraparticle diffusion, and liquid film diffusion [18]. Among them, electrostatic attraction is attributed to negatively charged biochar surfaces, which can adsorb positively charged groups that lose -OH after hydrolysis of BPA [22]. Surface diffusion may be related to the van der Waals force between the adsorbate BPA and the adsorbent WMB [21]. The intra-particle diffusion is mainly attributed to the mesoporous structure and surface characteristics of WMB, whose pore size is significantly larger than that of BPA molecules, so intra-particle diffusion is likely to exist in this adsorption process [37]. Liquid film diffusion is mainly caused by the concentration difference of the solvent BPA, so electrostatic attraction, surface diffusion, and intra-particle diffusion are the most important physical adsorption processes [20]. According to the characterization data of WMB, it can be inferred that the chemical adsorption of BPA mainly includes π-π bond interactions, hydrogen bonding, and ion or ligand exchange. Because WMB surfaces are rich in C=C/C-C bonds and aromatic and heterocyclic functional groups, which may vibrate in conjugation with the benzene ring of BPA to form π-π interaction. Additionally, the amino, methyl, or -COOH functional groups on WMB surfaces may form hydrogen bonds with the -OH groups of BPA. Finally, WMB may undergo a complexation reaction with BPA due to the many active sites on WMB surfaces, which are mainly manifested as phenolic hydroxyl groups at 3200 cm^{-1}. Phenolic hydroxyl groups are usually covalently bound and not ions on biochar, so their exchange is generally considered to be a ligand exchange process [37]. Similarly, the -COOH functional groups on the WMB surface may undergo exchange with the -OH groups in BPA, i.e., an ion exchange. Thus, these adsorption mechanisms are summarized in Figure 5. Since the focus of this study is not on a quantitative in-depth exploration of the adsorption mechanism of mask-based biochar, therefore, related research work is planned to be carried out in the future, mainly including the characterization and analysis of materials before and after adsorption, quantitative exploration of adsorption contribution, and molecular dynamics modeling.

3.6. Discussion of the Comparison with Hydrothermal Synthesis

3.6.1. Comparison of Hydrothermal Carbon Characterization and Adsorption Performance

Figure 6a and Figure S3a show the SEM images of HMB, which may be formed from flake-like or layered polyester fibers or other mask polymers. This is in obvious contrast to PMB, which is prepared by pyrolysis, and no microsphere structure is formed in the hydrothermal reaction. This may suggest that the hydrothermal reaction alone is not sufficient to completely carbonize the waste masks. Figure 6b,c show the SEM images of the HWMB. It can be seen that the blocky or flaky structures in this material may be derived from the carbon skeleton matrix after the hydrothermal carbonization of biomass. The scattered particles or chain-like microspheres on the surface (Figure S3b) are likely to be the products of the hydrothermal reaction of waste masks at high pressure. This suggests that a thermal polycondensation and cleavage process occurred between the waste masks (polypropylene and polyester fibers) and the biomass (natural polymers), which was attributed to the co-hydrothermal reaction providing the high temperature and pressure reaction conditions [38,39]. However, there is still a significant difference in the morphology of HWMB and WMB. The main feature is that the porous structure in the HWMB is not prominent and is filled or covered by chain-like microsphere particles. This may be caused by incomplete carbonization of the co-hydrothermal reaction, and the chain-like microsphere may be produced by polycondensation and polypropylene chain breakage, which is closely related to temperature [5,12]. Figure S3c shows the EDS analysis results of HMB. Compared with the results of HWMB (Figure 6d), the C content after co-hydrothermal carbonization is significantly reduced, but the O content is significantly increased. This may be attributed to the reaction of the polymer in the mask with the biomass at high temperature and pressure, with many carbon elements lost and added to the liquid, while the oxygen elements are fixed in the solid biochar. By comparing Figure 6d

and Table 1, there is a higher C content and lower N, O, and impurity content in WMB. This also shows that co-pyrolysis may provide a more thorough carbonization process and is more recommended for the disposal of waste masks.
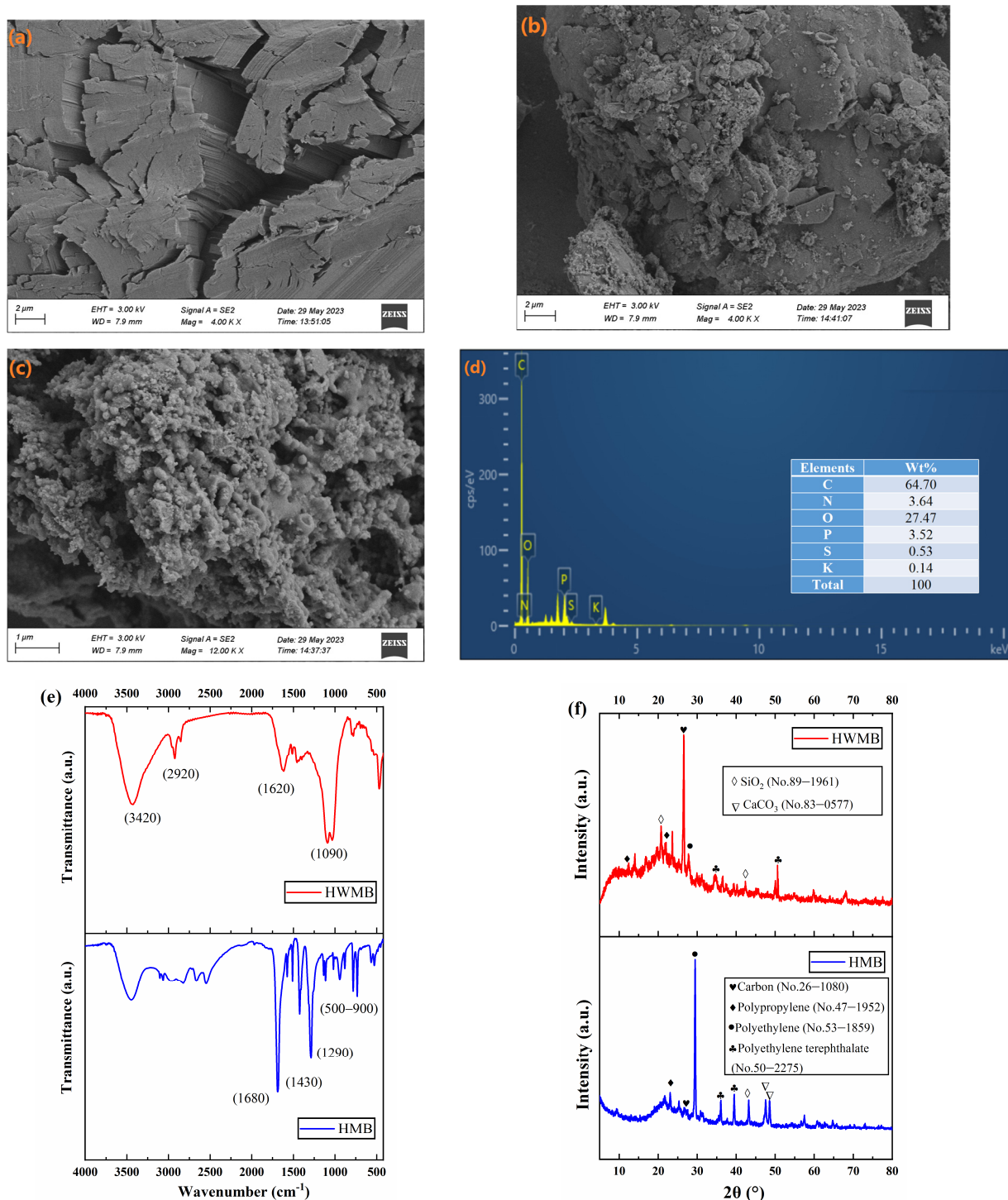

Figure 6. Material characterization of mask-based biochar prepared via hydrothermal synthesis: (**a**) SEM for HMB (magnified 4000 times), (**b**) SEM for HWMB (magnified 4000 times), (**c**) SEM for HWMB (magnified 12,000 times), (**d**) EDS for HWMB, (**e**) FTIR, and (**f**) XRD.

Figure 6e shows that the stretching vibration peak of the hydroxyl group (-OH) near 3420 cm^{-1} and the C-C/C=C resonance peak near 1090 cm^{-1} of HWMB are more obvious and higher in quantity than those of HMB. Moreover, with the addition of biomass to

the co-hydrothermal reaction, some heterocyclic, nitrogen-containing functional groups (-NH$_2$), and -COOH resonance peaks also began to transform. This suggests that the co-hydrothermal carbonization of waste masks is more efficient than a hydrothermal reaction alone. HWMB and WMB (Figure 3b) show no significant differences, and both have similar functional groups and proportions. The XRD (Figure 6f) characterization also confirms the above analysis results. HWMB was more thoroughly carbonization than HMB, which is evident from the more intensive carbon skeleton (JCPDS № 26-1080). Additionally, the extra SiO$_2$ (JCPDS № 89-1961) may come from impurities in the waste biomass, and CaCO$_3$ (JCPDS № 83-0577) may come from impurities in the waste masks or experimental waters. Polypropylene (JCPDS № 47-1952), polyethylene (JCPDS № 53-1859), polyethylene terephthalate (JCPDS № 50-2275), and ketone impurity peaks were similar to the crystals obtained by co-pyrolysis. It was also suggested that co-hydrothermal reactions could also synthesize biochar for masks.

Table S2 describes the specific surface area, pore volume, and pore size characteristics of the HWMB. Compared with the results of WMB (Table 1), there is a very small specific surface area of HWMB, only 0.85 m$^2 \cdot$g^{-1}. This may seriously affect the application prospects of HWMB, such as its adsorption performance. Figure 7 shows that both HWMB and WMB exhibit a clear trend of first increasing and then reaching equilibrium with the adsorption time increasing. This is also in line with the general law of adsorption kinetics [37]. However, regardless of the adsorption time, the adsorption capacity of BPA by WMB is significantly greater than that of HWMB, about 2.5 times. This also reflects that WMB has better adsorption performance than HWMB, owing to its material structure and physical–chemical properties. The fundamental reason might be that co-pyrolysis is more suitable than the co-hydrothermal method for preparing carbon materials with good performance from waste masks. In summary, the above comparative analysis of the physicochemical properties and adsorption performance confirms that WMB has better performance as a carbon material than HWMB. This validates the reasonableness of the co-pyrolysis method for disposing of waste mask resources recommended in this study and provides the necessary scientific data.
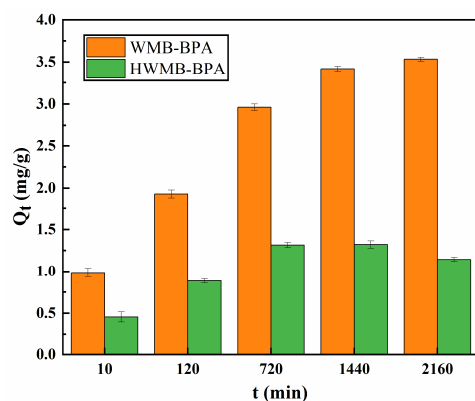

Figure 7. Comparison of the adsorption of BPA on mask-based biochar obtained by different preparation methods.

3.6.2. Comparison of the Bio-Oils Component

The bio-oil produced by hydrothermal alone and co-hydrothermal reactions was analyzed, and 62 peaks (matching 29 compounds) and 57 peaks (matching 26 compounds) were detected, respectively. These data are collated in Table 5, with compounds selected based on matching degree and peak area greater than 0.6. It can be seen that the bio-oil produced by the hydrothermal method has significantly fewer components than the pyrolysis method, and the chemical concentration is also relatively low. A classification of the substances in Table 5 shows that no heterocyclic compounds were identified, and the main components were aromatic and aliphatic compounds, with contents of 19.51% and

10.74%, respectively. The most abundant of these compounds is 1,4-Benzenedicarboxylic acid, bis(2-ethylhexyl) ester, with a peak area of 15.09%. This is the same as the highest component in the bio-oil produced by pyrolysis of pure waste masks, but the content is significantly lower than that produced by pyrolysis alone. It is a light yellow oily liquid with low toxicity and volatility. The second is 13-Docosenamide, (Z)-, with a peak area of 8.31%. It is commonly used as a softener and paper coating, providing anti-blocking properties and improving smoothness.

Table 5. The main components of bio-oils produced by the hydrothermal method were analyzed via GC-MS.

Corresponding Biochar Type	№	Library/ID	CAS №	Chemical Formula	Ret. Time (min)	Peak Area (%)
HMB	1	1,4-Benzenedicarboxylic acid, bis(2-ethylhexyl) ester	6422-86-2	$C_{24}H_{38}O_4$	29.196	15.09
	2	13-Docosenamide, (Z)-	112-84-5	$C_{22}H_{43}NO$	29.506	8.31
	3	Phthalic acid, di(2-propylpentyl) ester	- [a]	$C_{24}H_{38}O_4$	27.434	1.51
	4	4-Dehydroxy-N-(4,5-methylenedioxy-2-nitrobenzylidene)tyramine	-	$C_{16}H_{14}N_2O_4$	3.916	0.93
	5	(Z)-Docos-9-enenitrile	-	$C_{22}H_{41}N$	26.849	0.74
	6	Benzene, 1,3-dimethyl-	108-38-3	C_8H_{10}	3.674	0.64
	7	Dibutyl phthalate	84-74-2	$C_{16}H_{22}O_4$	21.265	0.61
HWMB	1	13-Docosenamide, (Z)-	112-84-5	$C_{22}H_{43}NO$	29.512	43.38
	2	1,4-Benzenedicarboxylic acid, bis(2-ethylhexyl) ester	6422-86-2	$C_{24}H_{38}O_4$	29.196	5.64
	3	(Z)-Docos-9-enenitrile	-	$C_{22}H_{41}N$	26.846	2.37
	4	cis-11-Eicosenamide	10436-08-5	$C_{20}H_{39}NO$	29.716	1.73
	5	9-Octadecenamide, (Z)-	301-02-0	$C_{18}H_{35}NO$	25.618	0.77
	6	Benzene, 1,3-dimethyl-	108-38-3	C_8H_{10}	3.990	0.75
	7	Phthalic acid, di(2-propylpentyl) ester	-	$C_{24}H_{38}O_4$	27.434	0.68

[a] This means the default CAS data.

Further analysis found that the hydrothermal reaction and co-hydrothermal reaction were very similar in terms of the composition of the bio-oil, and no heterocyclic compounds were detected. It contained a lot of aliphatic compounds (49.34%) and a few aromatic compounds (8.05%). The most abundant component is 13-Docosenamide, (Z)-, with a peak area of 43.38%. The bio-oil produced by hydrothermal synthesis also contains 1,4-Benzenedicarboxylic acid, bis(2-ethylhexyl) ester, with a peak area of about 5.64%. This is the opposite of the result of pure waste masks, indicating that biomass and waste masks can undergo sufficient hydrothermal reactions to further depolymerize the high molecular polymers, reducing the molecular weight of the liquid product [39]. At the same time, this may suggest that the co-hydrothermal process is more efficient than the carbonization of the hydrothermal process alone. Moreover, the composition of the bio-oil produced by hydrothermal reaction is relatively simple compared to that produced by pyrolysis, and the added value is not high. Therefore, co-pyrolysis is recommended for the efficient and thorough comprehensive utilization of waste masks and biomass resources.

3.7. Risk Assessment and Prospects

Some readers may wonder whether WMB, which is made from waste masks, has the potential to release secondary pollutants in water environment applications. Based on the organic matter leaching experiment and GC-MS tests [40], this study briefly evaluates the environmental application risk of WMB. The results show that WMB did not detect the leaching of polypropylene, polyethylene, and polyethylene terephthalate. These substances may be the most likely risk factors in the XRD (Figure 2a) characterization data. This also suggests that the preparation of carbon materials using waste masks as a carbon source may be green. Although the above substances were not detected, the environmental risk of

WMB in water treatment applications needs to be carefully evaluated through additional testing. Different carbonization conditions for waste masks also lead to differences in the structure of carbon materials, which can be prepared to include but not limited to amorphous carbon (such as activated carbon, carbon fiber, and carbon balls) and graphitic carbon nanomaterials (such as carbon nanotubes and graphene) [41]. In the future, it will be possible to develop polymer-derived carbon with the desired properties via the control of different carbonization conditions, such as high porosity, large specific surface area, functional and doping-induced surface properties, excellent electrical conductivity, and sufficient chemical stability. Biomass pyrolysis is an important technology for solving the problem of fossil energy, and many scholars have reached a consensus on this point [20]. To make more efficient use of waste masks and biomass resources, further research may be conducted on hydrogenation, catalytic cracking, or pyrolysis-catalytic upgrading in the future. This will increase the higher added value of bio-oil and pyrolytic gas, as well as the purity of the fuel for energy use. Additionally, catalysts can accelerate the pyrolysis reaction and regulate the product distribution, reducing the activation energy and reaction temperature of the reaction, thereby improving the efficiency of pyrolysis [26,34]. Moreover, modified catalysts may also be selected from materials such as metal ion-loaded molecular sieves with suitable pore structures and acidity [42,43]. Therefore, it is possible to develop corresponding catalysts to help the co-pyrolysis-catalytic upgrading reaction of waste masks and biomass. This may also be one of the research directions going forward.

4. Conclusions

To efficiently and comprehensively utilize waste masks and biomass waste resources, this study prepared mask-based biochar, bio-oil, and pyrolytic gas by the oxygen-limited co-pyrolysis method. The study found that waste masks participate in the co-pyrolysis process and shape the microspherical structure of biochar, increasing the types of surface functional groups, especially ester groups and aromatic heterocycles. Meanwhile, the specific surface area and pore volume of WMB also increased, improving the adsorption performance of BPA. As compared to the pyrolysis of pure masks, co-pyrolysis provides a more thorough carbonization reaction. The theoretical maximum adsorption capacity of WMB for BPA is 28.73 mg·g^{-1}, and the adsorption equilibrium is reached within 24 h, with an adsorption rate constant of 0.006 g·mg^{-1}·min^{-1}. The adsorption mechanisms are deduced to be related to physical–chemical interaction. Compared to the pyrolysis alone, the co-pyrolysis of bio-oil and pyrolytic gas not only increases the yield of aliphatic compounds but also reduces heterocyclic and aromatic compounds, thereby increasing resource efficiency and product-added value. These high value-added products could be used as potential fuels and chemical feedstocks in the pharmaceutical, food, and plastics industries. The co-pyrolysis mechanisms were discussed in detail, mainly involving the depolymerization of waste masks to produce a lot of aliphatic hydrocarbons and H radicals, which then undergo a multi-step low-polymerization reaction with the furan compounds formed by the depolymerization of hemicellulose and cellulose and the phenolic compounds formed by the depolymerization of lignin to produce a series of compounds. As compared to the hydrothermal reaction alone, the co-hydrothermal reaction also improves the quality of the biochar and bio-oil products. However, the solid products of co-pyrolysis have better physical–chemical properties and adsorption performance than hydrothermal carbon, and the liquid products have a richer composition and higher added value. WMB has not detected any pollutants that may be released, but the application risk still needs to be carefully assessed. In the future, it is hoped that the desired product may be better obtained by adding a catalyst for catalytic cracking or pyrolysis-catalytic upgrading. This study provides new perspectives for the efficient utilization of waste masks and contributes new insights for obtaining high value-added products by killing two birds with one stone.

Table S2: Specific surface area, pore volume, and pore size characteristics of HWMB; Figure S1: (a) Adsorption-desorption isotherm, (b) BJH-adsorption differential pore volume, and (c) cumulative pore volume/area-pore size distribution of WMB; Figure S2: Comparison of BPA adsorption by the prepared materials; Figure S3: SEM and EDS images. (a) SEM for HMB (magnified 10,000 times), (b) SEM for HWMB (magnified 10,000 times), and (c) EDS for HMB.

Author Contributions: T.W.: Conceptualization, methodology, software, data curation, supervision, project administration, and writing—first draft. D.Z.: Visualization and formal analysis. H.S.: Resources, supervision, and writing—review and editing. S.W., B.W., J.J., Z.F., W.Z. and Z.C.: Investigation and validation. D.Z.H.: Writing—review and editing. All authors have read and agreed to the published version of the manuscript.

Data Availability Statement: The data supporting the findings of this study are available within the article.

Conflicts of Interest: The authors have no relevant financial or non-financial interests to disclose.

References

1. Li, R.; Zhang, M.; Wu, Y.; Tang, P.; Sun, G.; Wang, L.; Mandal, S.; Wang, L.; Lang, J.; Passalacqua, A. What We Are Learning from COVID-19 for Respiratory Protection: Contemporary and Emerging Issues. *Polymers* **2021**, *13*, 4165. [CrossRef] [PubMed]
2. World Health Organization. Coronavirus Disease (COVID-19) Advice for the Public: When and How to Use Masks. 2020. Available online: https://www.who.int/emergencies/diseases/novel-coronavirus-2019/advice-for-public/when-and-how-to-use-masks (accessed on 1 August 2023).
3. Park, C.; Choi, H.; Lin, K.-Y.A.; Kwon, E.E.; Lee, J. COVID-19 mask waste to energy via thermochemical pathway: Effect of Co-Feeding food waste. *Energy* **2021**, *230*, 120876. [CrossRef] [PubMed]
4. Saberian, M.; Li, J.; Kilmartin-Lynch, S.; Boroujeni, M. Repurposing of COVID-19 single-use face masks for pavements base/subbase. *Sci. Total Environ.* **2021**, *769*, 145527. [CrossRef] [PubMed]
5. Yuwen, C.; Liu, B.; Rong, Q.; Zhang, L.; Guo, S. Porous carbon materials derived from discarded COVID-19 masks via microwave solvothermal method for lithiumsulfur batteries. *Sci. Total Environ.* **2022**, *817*, 152995. [CrossRef] [PubMed]
6. Jung, S.; Lee, S.; Dou, X.; Kwon, E.E. Valorization of disposable COVID-19 mask through the thermo-chemical process. *Chem. Eng. J.* **2021**, *405*, 126658. [CrossRef]
7. Wang, C.; Zou, R.; Lei, H.; Qian, M.; Lin, X.; Mateo, W.; Wang, L.; Zhang, X.; Ruan, R. Biochar-advanced thermocatalytic salvaging of the waste disposable mask with the production of hydrogen and mono-aromatic hydrocarbons. *J. Hazard. Mater.* **2022**, *426*, 128080. [CrossRef]
8. Silva AL, P.; Prata, J.C.; Walker, T.R.; Duarte, A.C.; Ouyang, W.; Barcelò, D.; Rocha-Santos, T. Increased plastic pollution due to COVID-19 pandemic: Challenges and recommendations. *Chem. Eng. J.* **2021**, *405*, 126683. [CrossRef]
9. Luo, Z.; Zhu, X.; Deng, J.; Gong, K.; Zhu, X. High-value utilization of mask and heavy fraction of bio-oil: From hazardous waste to biochar, bio-oil, and graphene films. *J. Hazard. Mater.* **2021**, *420*, 126570. [CrossRef]
10. Chen, S.; Liu, Z.; Jiang, S.; Hou, H. Carbonization: A feasible route for reutilization of plastic wastes. *Sci. Total Environ.* **2020**, *710*, 136250. [CrossRef]
11. Li, S.; Hu, J.; Aryee, A.A.; Sun, Y.; Li, Z. Three birds, one stone: Disinfecting and turning waste medical masks into valuable carbon dots for sodium hydrosulfite and Fe^{3+} detection enabled by a simple hydrothermal treatment. *Spectrochim. Acta A Mol. Biomol. Spectrosc.* **2023**, *296*, 122659. [CrossRef]
12. Abbas-Abadi, M.S.; Haghighi, M.N.; Yeganeh, H.; Mcdonald, A.G. Evaluation of pyrolysis process parameters on polypropylene degradation products. *J. Anal. Appl. Pyrolysis* **2014**, *109*, 272–277. [CrossRef]
13. Oginni, O. COVID-19 disposable face masks: A precursor for synthesis of valuable bioproducts. *Environ. Sci. Pollut. Res.* **2022**, *29*, 85574–85576. [CrossRef] [PubMed]
14. Emenike, E.C.; Iwuozor, K.O.; Agbana, S.A.; Otoikhian, K.S.; Adeniyi, A.G. Efficient recycling of disposable face masks via co-carbonization with waste biomass: A pathway to a cleaner environment. *Clean. Environ. Syst.* **2022**, *6*, 100094. [CrossRef]
15. Sari, M.M.; Inoue, T.; Salsabilla, V.C.; Septiariva, I.Y.; Mulyana, R.; Prayogo, W.; Arifianingsih, N.N.; Suhardono, S.; Suryawan, I.W.K. Transforming disposable masks to sustainable gasoline-like fuel via pyrolysis. *Environ. Adv.* **2024**, *15*, 100466. [CrossRef]
16. Shi, W.; Wang, H.; Yan, J.; Shan, L.; Quan, G.; Pan, X.; Cui, L. Wheat straw derived biochar with hierarchically porous structure for bisphenol A removal: Preparation, characterization, and adsorption properties. *Sep. Purif. Technol.* **2022**, *289*, 120796. [CrossRef]

17. Usman, A.; Ikhlas, S.; Ahmad, M. Occurrence, toxicity and endocrine disrupting potential of Bisphenol-B and Bisphenol-F: A mini-review. *Toxicol. Lett.* **2019**, *312*, 222–227. [CrossRef] [PubMed]

18. Godiya, C.B.; Park, B.J. Removal of bisphenol A from wastewater by physical, chemical and biological remediation techniques. A review. *Environ. Chem. Lett.* **2022**, *20*, 1801–1837. [CrossRef]

19. Wang, T.; Shi, H.; Kumar, A.; Zhang, D.; Wang, H.; Wang, S.; Zheng, J. Efficient visible-light photocatalysis of chloramphenicol using novel engineered biochar-based Ti-doped Bi_2WO_6 composite: Mechanisms, degradation pathways, and applications. *Sep. Purif. Technol.* **2024**, *332*, 125780. [CrossRef]

20. Zhang, D.; Wang, T.; Zhi, J.; Zheng, Q.; Chen, Q.; Zhang, C.; Li, Y. Utilization of Jujube Biomass to Prepare Biochar by Pyrolysis and Activation: Characterization, Adsorption Characteristics, and Mechanisms for Nitrogen. *Materials* **2020**, *13*, 5594. [CrossRef]

21. Wang, T.; Zheng, J.; Cai, J.; Liu, Q.; Zhang, X. Visible-light-driven photocatalytic degradation of dye and antibiotics by activated biochar composited with K^+ doped $g-C_3N_4$: Effects, mechanisms, actual wastewater treatment and disinfection. *Sci. Total Environ.* **2022**, *839*, 155955. [CrossRef]

22. Wang, T.T.; Zhang, D.; Fang, K.K.; Zhu, W.; Peng, Q.; Xie, Z.G. Enhanced nitrate removal by physical activation and Mg/Al layered double hydroxide modified biochar derived from wood waste: Adsorption characteristics and mechanisms. *J. Environ. Chem. Eng.* **2021**, *9*, 105184. [CrossRef]

23. Li, C.; Yuan, X.; Sun, Z.; Suvarna, M.; Hu, X.; Wang, X.; Ok, Y.S. Pyrolysis of waste surgical masks into liquid fuel and its life-cycle assessment. *Bioresour. Technol.* **2022**, *346*, 126582. [CrossRef] [PubMed]

24. Gebre, S.H.; Sendeku, M.G.; Bahri, M. Recent trends in the pyrolysis of non-degradable waste plastics. *ChemistryOpen* **2021**, *10*, 1202–1226. [CrossRef]

25. Zhang, Y.; Fu, Z.; Wang, W.; Ji, G.; Zhao, M.; Li, A. Kinetics, product evolution, and mechanism for the pyrolysis of typical plastic waste. *ACS Sustain. Chem. Eng.* **2021**, *10*, 91–103. [CrossRef]

26. Peng, Y.; Wang, Y.; Ke, L.; Dai, L.; Wu, Q.; Cobb, K.; Zeng, Y.; Zou, R.; Liu, Y.; Ruan, R. A review on catalytic pyrolysis of plastic wastes to high-value products. *Energy Convers. Manag.* **2022**, *254*, 115243. [CrossRef]

27. Cheng, L.; Gu, J.; Wang, Y.; Zhang, J.; Yuan, H.; Chen, Y. Polyethylene high-pressure pyrolysis: Better product distribution and process mechanism analysis. *Chem. Eng. J.* **2020**, *385*, 123866. [CrossRef]

28. Mahendra, R.A. Pyrolytic Product Distribution Analysis on Co-Pyrolysis of Face Mask Waste and Lignocellulosic Waste. *METAL J. Sist. Mek. Dan Termal* **2024**, *7*, 36–44.

29. Wang, G.; Dai, G.; Ding, S.; Wu, J.; Wang, S. A new insight into pyrolysis mechanism of three typical actual biomass: The influence of structural differences on pyrolysis process. *J. Anal. Appl. Pyrolysis* **2021**, *156*, 105184. [CrossRef]

30. Chen, X.; Che, Q.; Li, S.; Liu, Z.; Yang, H.; Chen, Y.; Wang, X.; Shao, J.; Chen, H. Recent developments in lignocellulosic biomass catalytic fast pyrolysis: Strategies for the optimization of bio-oil quality and yield. *Fuel Process. Technol.* **2019**, *196*, 106180. [CrossRef]

31. Wang, J.; Zhang, Z.K.; Jiang, J.C. A review on co-pyrolysis of biomass and waste plastics/rubbers. *J. For. Eng.* **2023**, *8*, 10–20.

32. Sharifzadeh, M.; Sadeqzadeh, M.; Guo, M.; Borhani, T.N.; Konda, N.M.; Garcia, M.C.; Wang, L.; Hallett, J.; Shah, N. The multi-scale challenges of biomass fast pyrolysis and bio-oil upgrading: Review of the state of art and future research directions. *Prog. Energy Combust. Sci.* **2019**, *71*, 1–80. [CrossRef]

33. Leng, E.; Guo, Y.; Chen, J.; Liu, S.; Jiaqiang, E.; Xue, Y. A comprehensive review on lignin pyrolysis: Mechanism, modeling and the effects of inherent metals in biomass. *Fuel* **2022**, *309*, 122102. [CrossRef]

34. Zhang, X.; Lei, H.; Chen, S.; Wu, J. Catalytic co-pyrolysis of lignocellulosic biomass with polymers: A critical review. *Green Chem.* **2016**, *18*, 4145–4169. [CrossRef]

35. Hassan, H.; Hameed, B.; Lim, J. Co-pyrolysis of sugarcane bagasse and waste high-density polyethylene: Synergistic effect and product distributions. *Energy* **2020**, *191*, 116545. [CrossRef]

36. Singh, M.; Salaudeen, S.A.; Gilroyed, B.H.; Al-Salem, S.M.; Dutta, A. A review on co-pyrolysis of biomass with plastics and tires: Recent progress, catalyst development, and scaling up potential. *Biomass Convers. Biorefinery* **2023**, *13*, 8747–8771. [CrossRef]

37. Wang, T.; Zheng, J.; Liu, H.; Peng, Q.; Zhou, H.; Zhang, X. Adsorption characteristics and mechanisms of Pb^{2+} and Cd^{2+} by a new agricultural waste–Caragana korshinskii biomass derived biochar. *Environ. Sci. Pollut. Res.* **2021**, *28*, 13800–13818. [CrossRef] [PubMed]

38. Fu, Z.; Zhang, Y.S.; Ji, G.; Li, A. Hydrothermal transformation behavior and degradation pathway analysis of waste surgical masks in supercritical water. *Process Saf. Environ. Prot.* **2023**, *176*, 776–785. [CrossRef]

39. Farru, G.; Libra, J.A.; Ro, K.S.; Cannas, C.; Cara, C.; Muntoni, A.; Piredda, M.; Cappai, G. Valorization of Face Masks Produced during COVID-19 Pandemic through Hydrothermal Carbonization (HTC): A Preliminary Study. *Sustainability* **2023**, *15*, 9382. [CrossRef]

40. Wang, T.; Cai, J.; Zheng, J.; Fang, K.; Hussain, I.; Husein, D.Z. Facile synthesis of activated biochar/$BiVO_4$ heterojunction photocatalyst to enhance visible light efficient degradation for dye and antibiotics: Applications and mechanisms. *J. Mater. Res. Technol.* **2022**, *19*, 5017–5036. [CrossRef]

41. Dai, L.; Zhou, N.; Lv, Y.; Cobb, K.; Cheng, Y.; Wang, Y.; Liu, Y.; Chen, P.; Zou, R.; Lei, H. Pyrolysis-catalysis for waste polyolefin conversion into low aromatic naphtha. *Energy Convers. Manag.* **2021**, *245*, 114578. [CrossRef]

42. Cai, N.; Li, X.; Xia, S.; Sun, L.; Hu, J.; Bartocci, P.; Fantozzi, F.; Williams, P.T.; Yang, H.; Chen, H. Pyrolysis-catalysis of different waste plastics over Fe/Al$_2$O$_3$ catalyst: High-value hydrogen, liquid fuels, carbon nanotubes and possible reaction mechanisms. *Energy Convers. Manag.* **2021**, *229*, 113794. [CrossRef]

43. Hidayat, A.; Dimas, D.; Sidiq, I. Co-Pyrolysis of Disposable Mask with Sugarcane Bagasse. *Mater. Sci. Forum* **2022**, *1073*, 161–166. [CrossRef]